Characterization and functional analysis of glycosylation in mouse pluripotent stem cells

マウス多能性幹細胞における網羅的糖鎖プロファイリングと機能解析

18D5603 Pecori Federico Supervisor Nishihara Shoko

要旨

マウス胚幹細胞細胞（ESCs）およびエピブラスト様細胞（EpiLCs）は、*in vitro*で胚の初期発生を再現する多能性幹細胞（PSCs）であり、ESCsであるナイーブ状態のPSCsからEpiLCsであるプライム状態のPSCsへの遷移メカニズムの解明を可能するモデルとなる。はじめに、ESCsとEpiLCsの網羅的糖鎖プロファイリングを行い、糖鎖構造が発生の初期段階から劇的な変化を遂げることを明らかにした。この変化は、クロマチンリモデラーであるpolycomb repressive complex 2 (PRC2)によって制御されており、全体の糖鎖構造を調節するネットワークの存在を見出した。さらに、ESCsにおける糖鎖の機能解析も行い、*O*-結合型でムチン型糖鎖の一種であるT抗原（Galβ1-3GalNAc）とその構造を合成するC1galt1がESCsの多能性の維持に関与していることを示した。本研究では、多能性の状態遷移中に発生する糖鎖のダイナミクスを明らかにし、糖鎖によるESCs多能性の制御メカニズムを特定した。

Keywords: pluripotent stem cells, glycomics, epigenetics, mucin-type *O*-glycosylation, Wnt signaling.

1. Background

Embryonic stem cells (ESCs) are pluripotent stem cells (PSCs) derived from pre-implantation embryos at E3.5-E4.5[1]. Epiblast-like cells (EpiLCs), which differentiate from ESCs in culture, resemble the embryo post-implantation stage at E5.5-E6.5[2]. ESCs and EpiLCs reflect two distinct pluripotent states known as the naïve state and the primed state, respectively, providing a useful *in vitro* model system to examine the pluripotent state transition occurring at embryo implantation *in vivo*[3].

To date, several signaling pathways involved in pluripotency regulation have been identified. Leukemia inhibitory factor (LIF) and bone morphogenic factor (BMP) signaling are strongly involved in the maintenance of ESC pluripotency via the LIF receptor and BMP receptor families, respectively[4,5]. In contrast, fibroblast growth factor (FGF) signaling triggers ESC differentiation into EpiLCs via the FGF receptor family[6]. Wingless-type (Wnt) signaling maintains the pluripotent state while at the same time priming cells for differentiation via interaction of Wnt ligands with Frizzled (Fzd) receptor family[7]. Indeed, induction of Wnt signaling by CHIR99021 (CHIR) together with the FGF signaling inhibitor PD0325901 (PD) is commonly used to maintain the undifferentiated state in cultured ESCs. However, CHIR alone induces ESC differentiation[8]. PSCs represent a promising tool to dissect the mechanisms underpinning mammalian development and advance regenerative medicine. Nevertheless, a significant number of attributes remain unexplored, hampering PSC exploitation.

Glycosylation, which is expected to be present on more than half of all mammalian proteins[9], is one of the most abundant post-translational modifications and is exerted by over 200 distinct glycosyltransferases and related enzymes in mammals. The overall glycomic profile has been characterized in mouse and human ESCs (hESCs), human induced pluripotent stem cells (hiPSCs), tumors and late differentiating cells[10–12]. Nonetheless, the glycosylation dynamics during mammalian early embryonic development remain unexplored.

Glycosylation is involved in a wide range of cellular processes, such as adhesion, signaling regulation, endocytosis, protein folding and protein stability[13]. To date, numerous studies have reported the critical role of glycosylation in development and stem cell regulation across different species[14,15]. Mucin-type *O*-glycosylation is an evolutionarily conserved protein modification and, together with *N*-linked glycosylation, is one of the most abundant forms of glycosylation present on membrane proteins and secreted proteins[16]. *O*-glycosylation is a stepwise process characterized by the initial attachment of *N*-acetylgalactosamine (GalNAc) to the hydroxyl group of serine or threonine residues of the target protein by a large family of 19 polypeptide α-*N*-acetylgalactosaminyltransferases (Galnts) in mouse; the attachment of GalNAc forms the so-called Tn antigen. Galactose (Gal), sialic acid (Neu5Ac), or *N*-acetylglucosamine (GlcNAc) can be successively added to Tn antigen by core 1 β1,3-galactosyltransferase (C1galT1), GalNAc α2,6-sialyltransferase-I (St6galnac1), and β1,3-*N*-acetylglucosaminyltransferase-6 (B3gnt6), to form three main structures: T antigen (Galβ1-3GalNAc), sialyl Tn antigen (NeuAcα2-6GalNAc), and Core 3 structure (GlcNAcβ1-3GalNAc), respectively[17]. Recently, a novel culture medium that includes the primitive growth factor $NME7_{AB}$, which binds to the

extracellular domain of the cleaved form of the mucin-type *O*-glycosylated protein MUC1, was shown to maintain human ESCs in an undifferentiated state[18], suggesting that mucin-type *O*-glycosylation is involved in ESC pluripotency network. However, the function of mucin-type *O*-glycosylation in ESC pluripotency and its molecular mechanism remains unknown.

2. Research goal

The present study was initiated to characterize the glycomic dynamics during mouse pluripotent state transition and clarify the role mucin-type *O*-glycosylation in ESC pluripotency network.

3. Methods

3-1. Cell culture

ESCs were cultured on mouse embryonic fibroblasts (MEFs) that were prepared from embryos at embryonic day 14.5 and inactivated with 10 μg mitomycin C (Sigma-Aldrich). ESCs were maintained in ESC medium consisting of DMEM (Gibco) supplemented with 15% fetal bovine serum (FBS) (Nichirei Biosciences), 1% penicillin/streptomycin (Gibco), 0.1 mM 2-mercaptoethanol (Gibco), 0.1 mM non-essential amino acids (Gibco) and 1000 U/mL LIF (Chemicon International).

To induce EpiLC differentiation, ESCs were seeded at low density in gelatin-coated 60-mm dishes containing ESC medium in the presence of 1 μM PD (Wako), 3 μM CHIR (Wako) and LIF. The following day, EpiLC induction was performed; ESCs were cultured in ESC medium without LIF for 24h. Subsequently, EpiLC medium, consisting of DMEM/F12 (Gibco) supplemented with 20% knockout serum replacement (KSR) (Gibco), 2 mM L-glutamine (Invitrogen), 1% penicillin/streptomycin (Gibco), 0.1 mM 2-mercaptoethanol (Gibco), 0.1 mM nonessential amino acids (Gibco), 30 ng/ml FGF2 (Wako) and 0.6 μM JAK inhibitor (JAKi) (Santa Cruz Biotechnology), was added. EpiLCs were collected for further analysis at 72h post-induction.

For galectin-3 (Lgals3) addition, ESCs were cultured in ESC medium (- FBS) for 2 hours before addition of 15 μg/mL Lgals3 for 30 minutes in ESC medium (- FBS).

3-2. Western blotting analysis

Cells were lysed with lysis buffer (50 mM Tris-HCl [pH 7.4], 150 mM NaCl, 1% Triton X-100, 5 mM EDTA, 1 mM Na3VO4, 10 mM NaF, and protease inhibitors). Protein samples were separated on an SDS polyacrylamide gel and transferred to polyvinylidene fluoride membranes (Millipore). After antibody (Ab) incubation the membranes were then washed and developed with ECL Plus reagents (GE Healthcare).

3-3. Real-time PCR analysis

Total RNA was extracted from cells using TRIzol reagent (Invitrogen) and reverse-transcribed using a Superscript II First Strand Synthesis Kit (Invitrogen) and oligo-dT primers. Real-time PCR was performed with an ABI PRISM 7700 Sequence Detection System (Applied Biosystems) and SYBR Green Master Mix (Roche). For *St6galnac1*, *C1galt1*, *B3gnt6*, and *Gapdh* copy number, a region of 80-1000 bp of the genes was inserted into a pGEM®-T easy vector (Promega). The vectors were linearized and a concentration ranging 100-0.01 pg/μL diluted in 1 μg/mL yeast tRNA was obtained by serial dilution to create a standard curve for each gene.

3-5. FACS profiling

A single cell suspension for cell surface molecules staining was obtained using 0.02% EDTA/PBS. Subsequently, 2-3 x 10^5 cells were collected and washed in FACS buffer (0.5% BSA (Iwai), 0.1% sodium azide (Sigma-Aldrich) in PBS). After washing, the cell suspension was incubated with Abs or lectins in FACS buffer. For internal molecules analysis, cells were harvested with 0.25% trypsin/EDTA (Thermo Fisher Scientific) and fixed/permeabilized for 30 min with 100% methanol (Wako) before staining. Samples were then analyzed using a BD FACSAria III Cell Sorter (Becton Dickinson).

3-6. *C1galt1* transient knockdown

For transient knockdown (KD) of *C1galt1* in ESCs, we generated small hairpin RNA (shRNA) expression vectors targeting two different regions of *C1galt1* (and also enhanced green fluorescent protein (Egfp) as the control) by inserting the appropriate double-stranded DNA between the BamH1 and HindIII sites of pSilencer 3.1-H1 (Ambion). Transfected cells were cultured for 4 days post transfection with 2 μg/mL puromycin (Sigma-Aldrich).

3-7. Pull-down assay and surface biotinylation assay

Cell lysate was diluted 10-fold with wash buffer (lysis buffer without Triton X-100). Pull-down assay was performed using streptavidin magnetic beads (Bio-Rad). The surface biotinylation assay was performed using the Pierce cell surface protein isolation kit (Thermo Scientific) following the manufacturer's instruction.

3-8. Luciferase assay

A shRNA expression vector targeting *C1galt1* (2 μg) was cotransfected with the reporter plasmid TOPFLASH (Upstate Biotechnology; 2 μg) or FOPFLASH (Upstate Biotechnology; 2 μg); pCH110 (GE Healthcare; 0.2 μg) was used as a control for transfection efficiency. Cells were lysed 4 days after transfection. Luciferase activity was measured by Dual-Light System (Applied Biosystems) and a Lumat LB9501 luminometer (Berthold).

3-7. Immunostaining

Cells were fixed with 4% paraformaldehyde in PBS and washed in PBS. The fixed cells were blocked with 1%BSA/PBS with 0.3% Triton X-100 for the analysis of intracellular molecules. Images were obtained using an LSM 700 confocal laser microscope (Carl Zeiss).

4. Results and Discussion

4-1. Induction of EpiLCs from ESCs.

To investigate the glycosylation dynamics occurring at the implantation stage, I induced differentiation of EpiLCs from ESCs (Figure 1A). Transcriptional analysis of EpiLCs by Real-time PCR showed a negligible change

in the pluripotency marker *Oct3/4*, whereas genes associated with the naïve state, such as *Nanog*, *Esrrb*, *Klf2*, *Klf4*, *Rex1* and *Tbx3* were strongly downregulated, together with a striking increase in the primed markers *Fgf5*, and *Otx2* (Figure 1B). Accordingly, Oct3/4 protein level was retained in EpiLCs at levels similar to those in ESCs, whereas the naïve marker Nanog decreased and the primed marker Otx2 increased. Furthermore, the phosphorylation level of ERK1/2, a downstream kinase involved in FGF signaling[6], was significantly higher in EpiLCs (Figure 1C), confirming the successful differentiation of EpiLCs from ESCs.

4-2. PRC2 contributes to glycosylation changes during ESC to EpiLC transition.

To obtain detailed insights into the glycome dynamics during the ESC to EpiLC transition, I performed a FACS profiling using a set of lectins that recognize glycan structures with different specificity. Strikingly, overall glycan structures underwent dramatic changes during the ESC differentiation into EpiLCs (Figure 2A). Since the glycosylation profile dynamically changes during ESC to EpiLC transition, I hypothesized the presence of a defined regulatory network. To identify putative candidates, an in-depth analysis of previously published chromatin immunoprecipitation sequencing (ChIP-seq) datasets obtained in ESCs was performed. This led to the identification of polycomb repressive complex 2 (PRC2), a chromatin-remodeling complex which deposits three methyl groups at histone H3 lysine 27 (H3K27me3) to promote gene repression[19]. Consistently, ESC treatment with the PRC2 inhibitor EED226 resulted in a large number of glycan structures alteration (Figure 2A). Comparison of EpiLCs and EED treated ESCs profiling led us to postulate the presence of at least three coordinated pathways that control glycosylation dynamics during EpiLC differentiation (Figure 2B).

These findings are the first demonstration that glycome complex alterations occurring during developmental transitions are orchestrated by a defined regulatory network. Consequently, it will be important to characterize the glycomic dynamics in a variety of developmental stages and cell types in order to identify transition-specific glycosylation regulatory components. Not surprisingly, aberrant forms of glycosylation are observed in all types of cancer[20]. Thus, I postulate the existence of glycosylation regulatory networks acting during tumorigenic processes, which identification will allow the development of novel therapeutic approaches.

4-3. *C1galt1* knockdown ESCs exit from pluripotency via Wnt signaling

I then focused on the functional analysis of mucin-type *O*-glycosylation, which role in ESC pluripotency network is unexplored. I analyzed mRNA expression in ESCs and found that *C1galt1* was the most highly expressed among *B3gnt6*, *C1galt1*, and *St6galnac1*, (Figure 3A,B). *C1galt1* KD resulted in reduction of the pluripotency markers Oct3/4 and Sox2 followed by upregulation of the Wnt signaling, as shown by the β-catenin luciferase reporter assay (Figure 3C-E). These data demonstrate that *C1galt1* KD cells spontaneously exit from pluripotency via excessive Wnt signaling, even in the presence of LIF.

4-4. T antigen on Frizzled-5 regulates its galectin-3-mediated endocytosis

Wnt signaling is initiated by the binding of the Wnt ligand to its receptor Fzd[7]. Among the Fzd receptor family involved in the β-catenin mediated Wnt signaling, Fzd5 is the most highly expressed in ESCs and plays an essential role during development[21]. A pull-down assay using biotinylated PNA, which specifically recognizes T antigen, in *C1galt1* KD ESCs followed by western blotting using an anti-Fzd5 Ab was performed. As a result, I found that the amount of Fzd5 protein precipitated in *C1galt1* KD cells decreased compared to the control, demonstrating that Fzd5 carries T antigen (Figure 3F). Mucin-type *O*-glycosylation has multiple functions, such as in protein-protein interaction, and in trafficking and turnover of cell surface proteins[13]. A surface biotinylation assay showed that Fzd5 was markedly increased on the surface of *C1galt1* KD cells (Figure 3G), indicating that T antigen on Fzd5 is involved in its endocytosis.

Galectins (Lgals) belong to a family of carbohydrate-binding proteins that bind to β-galactose-containing glycoproteins. Particularly, previous reports showed that Lgals3 can bind T antigen and have a stimulatory effect on endocytosis[22,23]. Therefore, I hypothesized that Lgals3 is involved in Fzd5 endocytosis. Consistently, addition of Lgals3 resulted in an enhancement of internalized Fzd5, confirming that Lgals3 is involved in Fzd5 endocytosis in ESCs (Figure 3H). In conclusion, these findings demonstrate that reduction of T antigen by *C1galt1* KD results in disruption of Lgals3-mediated endocytosis of the Wnt receptor Fzd5. The retention of Fzd5 on the surface, in turn, promotes excessive Wnt signaling activation via β-catenin, resulting in the exit from pluripotency (Figure 4).

It is becoming clear that glycosylation acts as a pivotal regulatory switch of pluripotency in a range of cell types in different organisms[15]. In the present study, I characterized glycosylation dynamics occurring during the mouse pluripotent state transition and clarified the function of mucin-type *O*-glycosylation in the pluripotency network in ESCs.

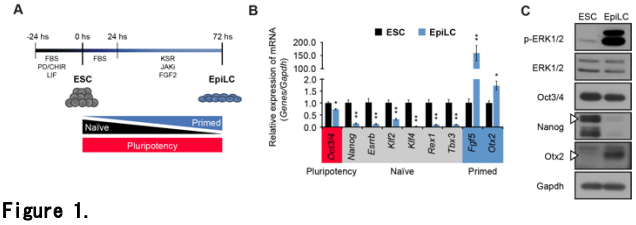

Figure 1.

A. Schematic representation of EpiLC differentiation protocol from ESCs. **B.** Real-time PCR analysis in ESCs and EpiLCs. **C.** Representative image of a western blot analysis in ESCs and EpiLCs. Values are shown as means ± s.e.m. of three independent experiments. Significant values are indicated as * $P < 0.05$, and ** $P < 0.01$.

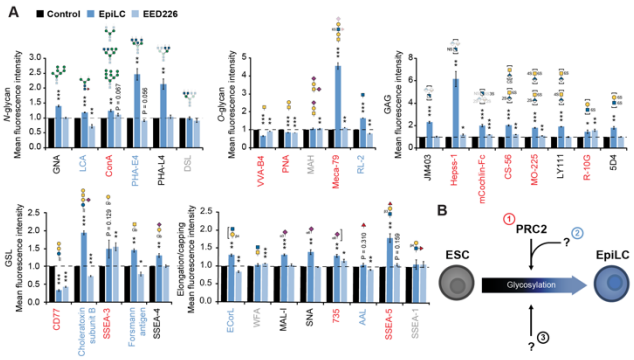

Figure 2.
A. Overall glycomic profiling by FACS using specific lectins/Abs in EpiLCs and EED226-treated ESCs, shown as a fold change relative to ESCs and DMSO-treated ESCs (control), respectively. **B.** Schematic representation of the glycosylation regulatory network during ESC to EpiLC transition. Values are shown as means ± s.e.m. of three independent experiments. Significant values are indicated as * $P < 0.05$, ** $P < 0.01$, and *** $P < 0.001$.

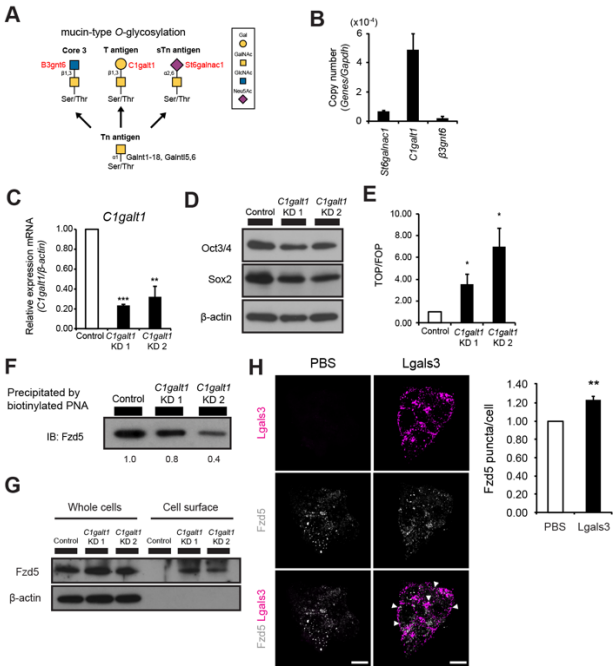

Figure 3.
A. Schematic diagram of mucin-type *O*-glycosylation pathway initial step. **B.** *Genes* copy numbers normalized to that of *Gapdh*. **C.** Real-time PCR analysis in *C1galt1* KD ESCs. **D.** Representative image of a western blot analysis of pluripotent markers in *C1galt1* KD cells. **E.** Luciferase assay of *C1galt1* KD cells. The relative light unit amount is shown as a ratio of TOPFLASH/FOPFLASH normalized against β-galactosidase. **F.** Representative image of a western blot (IB) using an anti-Fzd5 Ab on the lectin precipitated fraction precipitated with biotinylated PNA in *C1galt1* KD cells. **G.** Assessment of Fzd5 surface protein in *C1galt1* KD cells using a surface biotinylation assay. **H.** Representative image of a maximum intensity projection of intracellular molecules in ESCs treated with recombinant Lgals3 and related Fzd5 puncta quantification. Arrowheads indicate colocalization of Fzd5 puncta and Lgals3. Scale bar, 10 μm. The values are shown as means ± s.e.m. of three independent experiments. Significant values are indicated as * $P < 0.05$, ** $P < 0.01$, and *** $P < 0.001$.

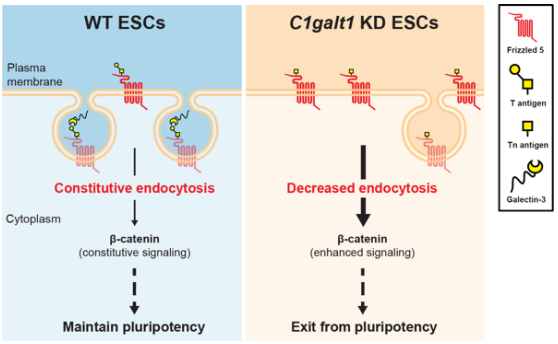

Figure 4.
Schematic representation of ESC pluripotency regulation by mucin-type *O*-glycosylation.

5. References

1. Evans M.J. & Kaufman M.H. *Nature* **292**, 154-156 (1981).
2. Hayashi K., Ohta H., Kurimoto K., Aramak, S. & Saitou M. *Cell* **146**, 519-532 (2011).
3. Nichols J. & Smith A. *Cell Stem Cell* **4**, 487-492 (2009).
4. Niwa H., Ogawa K., Shimosato D. & Adachi K. *Nature* **460**, 118-122 (2009).
5. Ying Q.L., Nichols J., Chambers I. & Smith A. *Cell* **115**, 281-292 (2003).
6. Lanner F. & Rossant J. *Development* **137**, 3351-3360 (2010).
7. ten Berge D. *et al. Nat. Cell. Biol.* **113**, 1070-1075 (2011).
8. Ying Q.L. *et al. Nature* **453**, 519-523 (2008).
9. Apweile R., Hermjakob H. & Sharon N. *Biochim. Biophys. Acta* **1473**, 4-8 (1999).
10. Nairn A.V. *et al. J. Biol. Chem.* **287**, 37835-37856 (2012).
11. Fujitani N. *et al. Proc. Natl. Acad. Sci. USA* **110**, 2105-2110 (2013).
12. Homan K. *et al. Int. J. Mol. Sci.* **20**, pii: E3546 (2019).
13. Varki A. *Glycobiology* **27**, 3-49 (2017).
14. Haltiwange R.S. & Lowe J.B. *Annu. Rev. Biochem.* **73**, 491-537 (2004).
15. Nishihara S. *FEBS Lett.* **592**, 3773-3790 (2018).
16. Tran D.T. & Ten Hagen K.G. *J. Biol. Chem.* **288**, 6921-6929 (2013).
17. Bennet E.P. *et al. Glycobiology* **22**, 736-756 (2012).
18. Carter M.G. *et al. Stem Cells* **34**, 847-859 (2016).
19. Gökbuget D. & Blellock R. *Development* **146**, pii: dev164772 (2019).
20. Pinho S.S. & Reis C.A. *Nat. Rev. Cancer* **15**, 540-555 (2015).
21. Hao J., Li T.G., Qi X., Zhao D F. & Zhao G. Q. *Dev. Biol.* **290**, 81-91 (2006).
22. Johannes L., Jacob R. & Leffler H. *J. Cell. Sci.* **131**, jcs208884 (2018).
23. Lepur A. *et al. Biochim. Biophys. Acta.* **1820**, 804-818 (2012).